Monteiro *et al. Appl Adhes Sci (2015) 3:25*
DOI 10.1186/s40563-015-0056-y

Applied Adhesion Science
a SpringerOpen Journal

RESEARCH Open Access

Experimental estimation of the mechanical and fracture properties of a new epoxy adhesive

J. P. R. Monteiro[1], R. D. S. G. Campilho[1*], E. A. S. Marques[2] and L. F. M. da Silva[3]

*Correspondence:
raulcampilho@gmail.com
[1] Departamento de Engenharia Mecânica, Instituto Superior de Engenharia do Porto, Instituto Politécnico do Porto, Rua Dr. António Bernardino de Almeida, 431, 4200-072 Porto, Portugal
Full list of author information is available at the end of the article

Abstract

The automotive industry is currently increasing its use of high performance structural adhesives in order to reduce vehicle weight and increase the crash resistance of automotive structures. To achieve these goals, the high performance adhesives employed in the automotive industry must not only have high mechanical strength but also large ductility, enabling them to sustain severe dynamic loads. Due to this complex behaviour, the design process necessary to engineering structures with these materials requires a complete knowledge of their mechanical properties. In this work, the mechanical properties of a structural epoxy, Sikapower® 4720, were determined. Tensile tests were performed to determine the Young's modulus (E) and tensile strength (σ_f). Shear tests were performed to determine the shear modulus (G) and the shear strength (τ_f). Tests were also performed to assess the toughness of the adhesive. For mode I toughness determination (G_{Ic}), the double-cantilever beam (DCB) test was employed. For determination of toughness under mode II (G_{IIc}), the end-notched flexure (ENF) test was performed. The data obtained from the DCB and ENF tests was analysed with the compliance calibration method (CCM), corrected beam theory (CBT) and compliance-based beam method (CBBM) techniques. The test results were able to fully mechanically characterize the adhesive and demonstrate that the adhesive has not only high mechanical strength but combines this with a high degree of ductility, which makes it adequate for use in the automotive industry.

Keywords: Structural adhesive, Bulk specimens, Thick adherend shear test, Fracture toughness

Background

The reduction of structural weight and the enhancement of vehicle safety are currently two of the most important research subjects for the automotive industry. The demand for lighter and safer structures has led the designers to increasingly employ alternative joining methods, replacing the more commonly used spot welding. Adhesive bonding is one of these methods and its use has expanded significantly, driven by the development of improved high performance adhesives and bonding techniques. While previous adhesives were relatively strong but brittle, the adhesives currently used for structural bonding by the automotive industry are designed with the aim of providing the joint with high ductility and high mechanical strength [1]. These materials are commonly referred

as crash resistant adhesives due to their ability to plastically deform but still maintain the structure firmly bonded under significantly large loads, therefore ensuring that the structure has a large degree of energy absorption. Modern automotive structures combine multiple bonded materials and use adhesive layers with complex geometry. To efficiently design such structures, the use of finite element method (FEM) techniques is fundamental. One of the most accurate methods to model adhesive layers are cohesive zone models (CZM) to simulate adhesive failure and associated debonding. CZM are a very powerful tool for studying the behavior of adhesive joints. Cohesive elements can be easily added to FEM models. Needleman [2], Tvergaard et al. [3] and Camacho et al. [4] were among the first to adapt this technique for use in adhesive joints. A CZM improves on classical continuum mechanics modelling and can describe the fracture process and location. By using both strength and energy parameters to simulate the nucleation and advance of a fracture crack [5], these elements can fully simulate the crack progression in adhesive layers. The relationship between the stresses and displacements is governed by a traction separation law.

The experimental campaign described in this work enabled the estimation of E, G, σ_f, τ_f, G_{Ic} and G_{IIc}. The tensile properties of the specimen (E and σ_f) were determined using the bulk tensile testing of "dog bone" specimens. This almost universal test is standardized under ISO 527:1997 [6] and its ASTM equivalent D638-03 [7]. To measure the shear properties of the adhesive (G and τ_f), the thick adherend shear test (TAST) was employed. This test follows the standard ISO 11003-2:1993 [8]. Another method commonly employed to assess τ_f of adhesives is the torsion test, standardized under ASTM E143-02 [9]. The determination of G_{Ic} is usually performed with the DCB specimen [10], although other common specimen geometries exist such as the tapered double-cantilever beam (TDCB) or the single edge notch bend (SENB) specimens. The DCB test is widely used because it requires relatively simple specimens and it has well defined testing procedures. Several methodologies exist that allow the derivation of G_{Ic} from this testing data, resulting from a linear elastic fracture mechanics analysis. During a DCB test it is assumed that a crack will stably propagate when the tensile strain energy release rate (G_I) equals G_{Ic}. The CCM is based on the Irwin-Kies [11] equation and requires the calculation of the compliance (C) relatively to the crack length (a). The compliance is given by $C = \delta/P$, where δ is the displacement and P is the applied load. As an alternative, the DBT uses the classical beam theory equations to assess the compliance [12] and the CBT improves on it by taking account the effects of crack tip rotation and deflection [13]. All these methods require the constant measurement of the crack location, which might be difficult or yield imprecise results. As an alternative, the CBBM uses the concept of the crack equivalent [14]. This means that it derives the crack location solely from C at any given moment, negating the need to visually monitor the crack progression as required by other methods [15]. The determination of G_{IIc} can be performed using three different tests by the theoretically steady-state value of shear strain energy release rate (G_{II}) that is attained during crack propagation. The ENF test, the end-loaded split (ELS) and the four point end-notched flexure (4ENF) test. Among these alternatives, the ENF is the most commonly used, as it does not exhibit the friction problems found in the 4ENF test and avoids the excessively large displacements found in the ELS test. The ENF has also the advantage of using a specimen mostly similar to the one used in the DCB

tests, differing only in the loading direction. The ENF test is simply a three-point flexure test on a pre-cracked specimen. During the ENF test the relative displacement of the upper and lower specimens introduces a shearing load in a pre-cracked adhesive layer. The data from these tests can be analyzed using the same methods used for the analysis of the DCB test results.

Saldanha et al. [16] have used similar methods to perform a characterization procedure on a high elongation, high toughness epoxy adhesive. They found that such adhesive combined the high tensile strength and shear strength typical of epoxy adhesives with the high toughness of polyurethane adhesives. Similarly, García et al. [17] characterized a toughened epoxy adhesive to use in the FEM. Their experimental procedure used only tensile and shear tests to build a continuum damage model that was able to accurately simulate the mechanical behavior of complete joints. Much of the work on characterizing toughened, high elongation epoxy adhesives focuses on the study of the fracture properties, where there are significant improvements to be found. A variety of specimen types are used in these tests. Jin et al. [18] studied the mode I fracture behavior of a self-healing toughened adhesive by the TDCB test. Kim et al. [19] performed a similar characterization for a nanoparticle reinforced epoxy but used the simpler single SENB specimens for this purpose. All these tests found improvements in toughness over standard epoxy formulations.

In this work, the mechanical properties of a structural epoxy, Sikapower® 4720, were determined. Tensile tests were performed to determine E and σ_f. Shear tests were performed to determine G and τ_f. Tests were also performed to assess the toughness of the adhesive. For G_{Ic} characterization, the DCB test was employed. For determination of G_{IIc}, the ENF test was performed. The data obtained from the DCB and ENF tests was analysed with the CCM, CBT and CBBM techniques. Comparison of the Sikapower® 4720 with another epoxy adhesive was also undertaken. The Araldite® 2015 was chosen for this purpose because of being a direct competitor in terms of applications and being established in the market. With this work, complete data for the numerical design of bonded structures with this novel adhesive is provided, enabling the optimization of the joints and the subsequent cost and weight reduction of the structures.

Methods

Tensile tests

Figure 1 shows the specimen dimensions for the bulk specimens with dogbone shape for tensile testing, which were fabricated according to the French Standard NF T 76-142 [20]. Curing of the specimens was carried out in a steel mold [21] that permits the simultaneous production of 6 specimens (Fig. 2). The top and bottom plates of the mold were machined by computer numerical control (CNC), and then grinded (to improve the surface finish) and hard chrome plated (to increase the abrasion resistance and facilitate demolding). The mold plate, to be placed between the top and bottom plates to produce the adhesive cavities, was laser cut. Before application of the adhesive, the mold was cleaned with acetone and demolding agent was applied. The adhesive was applied in the mold cavities by the application gun and manually spread, before being left for cure during 1 week. The tensile tests were performed in an Instron® 3367 testing machine with a 30 kN load cell, at room temperature and under displacement control (2 mm/min).

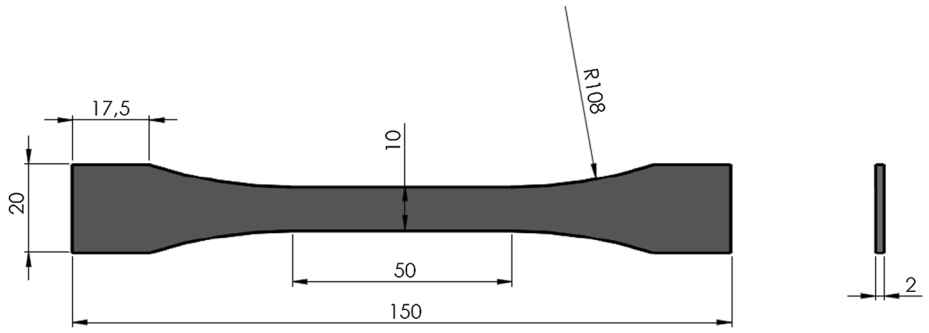

Fig. 1 Dimensions of the bulk adhesive specimens (in mm) by the French Standard NF T 76-142 [20]

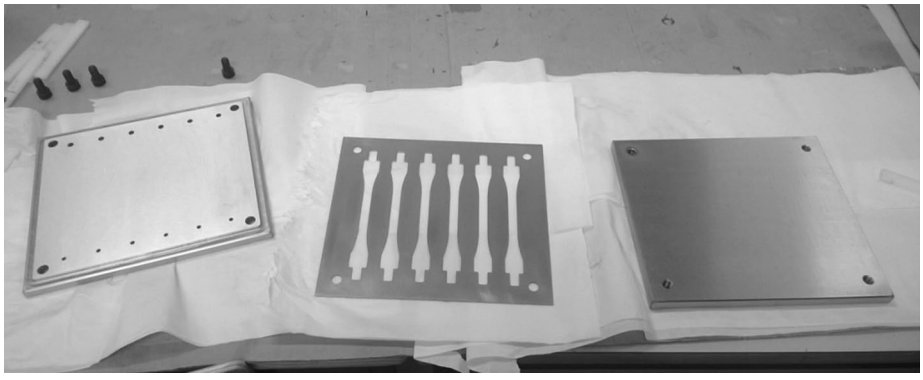

Fig. 2 Different constituents of the mold for fabrication of the bulk specimens

During the tests, the longitudinal strains (ε) were measured with a mechanical extensometer with a base length of 25 mm.

For the determination of the bulk tensile mechanical properties of the adhesive, the standard EN ISO 527-2 [6] was considered. E was measured between values of ε of 0.05 and 0.25 % as

$$E = \frac{\Delta\sigma}{\Delta\varepsilon}, \tag{1}$$

where $\Delta\sigma$ and $\Delta\varepsilon$ are the variations of tensile stress and strain, respectively. The yield stress (σ_y) was obtained for $\varepsilon = 0.2$ %, by the intercept between the tensile stress (σ)–ε curve and a parallel line to the initial part of this curve. σ_f is calculated by the ratio between the maximum load and the initial cross section of the sample. During the test, the tensile failure strain (ε_f) was also registered, corresponding to the maximum displacement sustained by the specimen.

Shear tests

The TAST was selected to perform the shear tests, using the adherends and machine gripping tools developed by Morais [22] in DIN C45E steel. All aspects related to the tests (e.g. geometry and dimensions) followed the ISO 11003-2 standard [8]. Surface preparation of

the steel adherends consisted of grit blasting and cleaning with acetone. The adherends were cured in a jig (Fig. 3) that ensures the precise alignment of the adherends and correct overlap length. The specimens were assembled using 1 mm spacers between adherends to attain the correct value of overlap length. These spacers and all the mounting jig surfaces potentially in contact with the adhesive were coated with demolding agent to facilitate extraction of the specimens after curing. Application of the adhesive was done manually (Fig. 4a), followed by manual positioning of the adherends with application of pressure on the joints (Fig. 4b). The limiting bars were then fastened to the jig to assure the correct overlap length and the specimens left to cure for 1 week at room temperature. The longitudinal strains during the test were measured with a mechanical extensometer. Figure 5 represents the test setup. The considered test speed was 0.5 mm/min (ISO 11003-2 standard [8]).

The ISO 11003-2 standard [8] was considered to determine the shear mechanical properties of the adhesive by TAST tests. The shear stress (τ) was calculated using the following equation

$$\tau = \frac{P}{l \times B}, \tag{2}$$

where l is the bond length and B is the specimens' width. The expression used to calculate the shear strain (γ) is given by

$$\gamma = \frac{\delta}{t_{\mathrm{A}}}, \tag{3}$$

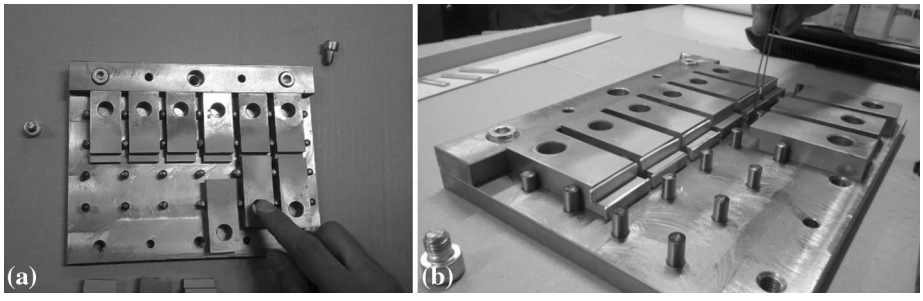

Fig. 3 Adherents placing in the jig: alignment of the adherends (**a**) and placement of the spacers (**b**)

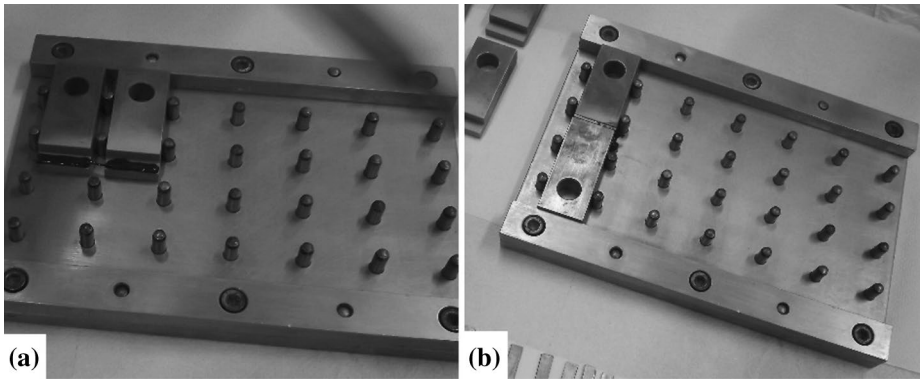

Fig. 4 Manufacturing of the TAST specimens: applying the adhesive (**a**) and adherends' positioning in the jig (**b**)

Fig. 5 TAST specimen attached to the testing machine with the mechanical extensometer

where t_A is the adhesive thickness. Subsequently, the value of G was determined in the elastic portion of the τ–γ curve as

$$G = \frac{\tau}{\gamma}. \tag{4}$$

Fracture tests

DCB tests were considered to calculate G_{Ic}, and ENF tests to obtain G_{IIc}. Both test methods used AA6082 T651 aluminum alloy adherends with the dimensions of $140 \times 25 \times 3$ mm^3 (DCB tests) and $230 \times 25 \times 3$ mm^3 (ENF tests). Previous characterization of this material in bulk tension [23] resulted in the following mechanical properties: $E = 70.07 \pm 0.83$ GPa, $\sigma_y = 261.67 \pm 7.65$ MPa, $\sigma_f = 324 \pm 0.16$ MPa and $\varepsilon_f = 21.70 \pm 4.24$ %. Figure 6 depicts the geometry and relevant dimensions of the DCB (a) and ENF specimens (b). The dimensions for the DCB joint are: total length $L = 140$ mm, initial crack length $a_0 \approx 55$ mm, adherend thickness $t_P = 3$ mm, $B = 25$ mm and $t_A = 0.2$ mm. The dimensions of the ENF specimens are: mid-span $L = 100$ mm, $a_0 \approx 60$ mm, $t_P = 3$ mm, $B = 25$ mm and $t_A = 0.2$ mm. The specimens were fabricated in a laboratory with controlled temperature and humidity. The bonding faces were prepared by grit blasting with corundum sand, cleaned with acetone and assembled in a steel mould for bonding. To obtain a constant value of t_A throughout the bonded portion of the specimens, calibrated steel spacers were inserted between the adherends, after proper preparation with demoulding agent. Moreover, at the crack tip, a sharp pre-crack was induced by a 0.1 mm thick razor blade between the calibrated steel spacers. After applying the adhesive, the specimens were closed following the best practices to avoid air entrapment and appearance of air bubbles within the adhesive layer. Curing was

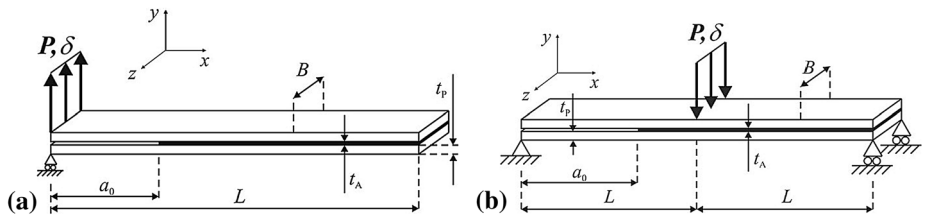

Fig. 6 Geometry and dimensions of the DCB (**a**) and ENF (**b**) specimens

performed at room temperature. Preparation for testing consisted of removing the steel spacers, spraying the adherends' sides with brittle white paint to enable a clear identification of a, and gluing a black numbered scale in both adherends to aid the a measurement. The testing programme involved testing six DCB and eight ENF specimens at room temperature using an Instron® 3367 electro-mechanical testing machine equipped with a 30 kN load cell. Images were captured during the tests using an 18 MPixel digital camera with no zoom and fixed focal distance to approximately 100 mm, which enabled obtaining the values of a with accuracy. The values of a were then correlated with the P-δ data by the time elapsed since the beginning of each test.

The value of G_{Ic} was evaluated by three data reduction schemes: the CCM, the CBT and the CBBM. The classical reduction schemes to estimate G_{Ic} are usually based on compliance calibration or the beam theory. The CCM is based on the Irwin-Kies equation [11]

$$G_{Ic} = \frac{P^2}{2B}\frac{dC}{da}, \tag{5}$$

where $C = \delta/P$. Cubic polynomials ($C = C_3a^3 + C_2a^2 + C_1a + C_0$) were used to fit the $C = f(a)$ curves, leading to

$$G_{Ic} = \frac{P^2}{2B}\left(3C_3a^2 + 2C_2a + C_1\right). \tag{6}$$

Beam theories were also used to measure G_{Ic}. Using the CBT, G_{Ic} is obtained using [24]

$$G_{Ic} = \frac{3P\delta}{2B(a + |\Delta|)}, \tag{7}$$

where Δ is a crack length correction for crack tip rotation and deflection, obtained as specified in the standard ISO 15024 [25]. The CBBM is a relatively straightforward but robust method, based on an equivalent crack length (a_{eq}), and it only depends on the specimen's compliance during the test. Applied to the DCB test specimen, it gives

$$G_{Ic} = \frac{6P^2}{B^2t_P}\left(\frac{2a_{eq}^2}{t_P^2E_f} + \frac{1}{5G_{AD}}\right). \tag{8}$$

Detailed explanations of the method can be found in the work of Campilho et al. [26]. The value of a_{eq} is estimated from the current specimen compliance and taking into

consideration the damage zone, E_f is a corrected flexural modulus to account for stress concentrations at the crack tip and stiffness variability between specimens, and G_{AD} is the shear modulus of the adherends.

The following techniques were tested for the ENF specimen: CCM, CBT and CBBM [27]. The classical data reduction schemes to obtain G_{IIc} are usually based on compliance calibration or beam theories. The CCM is based on the Irwin-Kies equation [28]

$$G_{IIc} = \frac{P^2}{2B}\frac{dC}{da}. \tag{9}$$

Cubic polynomials ($C = C_1a^3 + C_0$) were used to fit the $C = f(a)$ curves, resulting into

$$G_{IIc} = \frac{3P^2C_1a^2}{2B}. \tag{10}$$

Beam theories were also used to measure G_{IIc}. The CBT, which accounts for crack length corrections to consider the effects of shear deformation, was proposed by Wang and Williams [29] and is written as

$$G_{IIc} = \frac{9(a + 0.42\Delta_1)^2P^2}{16B^2E_xt_p^3}, \tag{11}$$

where E_x is the adherends E value in the length direction and Δ_1 is a crack length correction to account for shear deformation [27]

$$\Delta_I = t_p\sqrt{\frac{E_x}{11G_{xy}}\left[3 - 2\left(\frac{\Gamma}{1+\Gamma}\right)^2\right]}, \tag{12}$$

in which G_{xy} is the in-plane shear modulus of the adherends and Γ is given by

$$\Gamma = 1.18\sqrt{\frac{E_xE_y}{G_{xy}}}, \tag{13}$$

where E_y is the value of E of the adherends in the thickness direction. The CBBM was also developed for the ENF specimen [27], enabling the estimation of G_{IIc} only using the experimental compliance. This technique relies on a_{eq}, which is computed based on the current specimen's compliance and accounts for the fracture process zone (FPZ) effects at the crack tip (not taken into account when the real value of a is considered). G_{IIc} can be obtained by the following expression

$$G_{IIc} = \frac{9P^2a_{eq}^2}{16B^2E_ft_p^3}. \tag{14}$$

Detailed explanations of the method can be found in Ref. [27]. Equally to the DCB tests, E_f is an equivalent flexural modulus obtained from the specimen's initial compliance and value of a_0.

Results and discussion

Tensile tests

Figure 7 shows the σ–ε curves of the six bulk tensile tests, revealing the high repeatability of the results, apart from some deviations in the value of ε_f. All failures were smooth without voids or porosities. Table 1 summarizes the tensile mechanical properties of the bulk tests to the adhesive Sikapower® 4720 (P_{max} and δ_{max} are the maximum load and the maximum displacement, respectively).

In the present work, $\sigma_f = 27.519 \pm 0.845$ MPa was found for the Sikapower® 4720, slightly higher than the manufacturer's value of 24 MPa. However, the percentile standard deviation of only 3.1 % clearly shows the repeatability of the results obtained. Possible causes for this discrepancy are different curing parameters (time and/or temperature) or test protocol. The value of ε_f (1.973 ± 0.343 %) was smaller than that postulated by the manufacturer (3 %). This difference can be related to small fabrication defects that would prevent the full plasticity of the adhesive to develop in the bulk tests. On the other hand, E was higher that the reference value (2052.477 ± 84.818 MPa against 1900 MPa, respectively). The curing conditions, testing temperature and humidity, and also method used to estimate E may be on the origin of this difference. σ_y is not available for comparison.

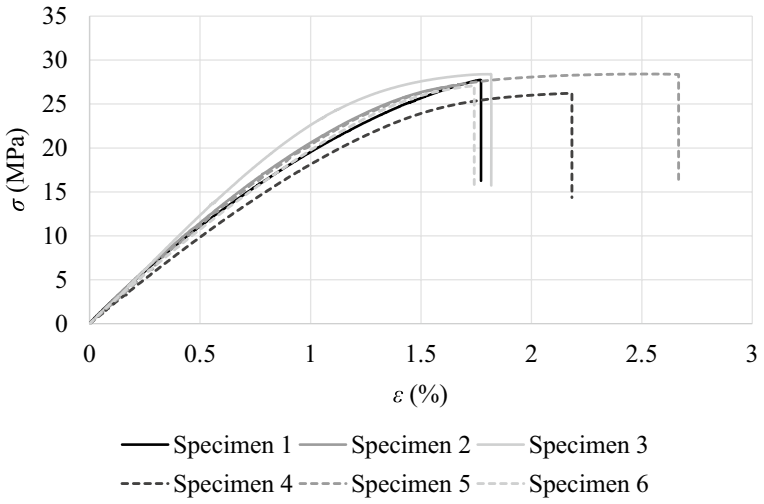

Fig. 7 σ–ε curves obtained for the six bulk tests

Table 1 Bulk mechanical properties in tension of the adhesive Sikapower® 4720

Specimen	P_{max} (N)	δ_{max} (mm)	σ_y (MPa)	σ_f (MPa)	ε_f (%)	E (MPa)
1	822.512	1.428	22.600	27.746	1.762	2162.285
2	886.882	1.861	20.048	27.212	1.755	2013.104
3	840.769	1.690	26.366	28.399	1.815	1988.688
4	822.810	1.943	21.979	26.228	2.183	1992.987
5	842.490	2.265	25.030	28.420	2.584	2160.623
6	803.614	1.755	23.691	27.109	1.741	1997.173
Average	836.513	1.824	23.286	27.519	1.973	2052.477
Standard deviation	28.485	0.279	2.252	0.845	0.343	84.818

Table 2 evaluates the tensile mechanical properties of the Sikapower® 4720 with another epoxy adhesive, the Araldite® 2015 [30]. Comparing the two adhesives, the Sikapower® 4720 excels in σ_f, E and σ_y, while the Araldite® 2015 has a higher value of ε_f.

Shear tests

Figure 8 presents the τ–γ curves of the adhesive Sikapower® 4720. Identically to the previous analysis, a high repeatability between specimens is found regarding the elastic stiffness, shear strength and ductility (except for specimen 1, which showed a significantly smaller value of maximum shear strain, γ_f, possibly due to fabrication related issues). The values of γ_f were calculated from the sharp drop of the load sustained by the specimens immediately before complete failure. Figure 9 represents the followed procedure to calculate the shear yield stress (τ_y), using the intercept between the τ–γ curve and a line parallel with the same initial slope of the τ–γ curve but offset by $\gamma = 0.2$ %. All failures were cohesive in the adhesive layer. Table 3 presents the collected shear mechanical properties from the TAST tests to the adhesive Sikapower® 4720. There is generally a good correspondence between specimens for each measured property, with a standard deviation below 10 %. Only for δ_{max} (37.1 %) and γ_f (34.0 %) this was not observed. The deviations between specimens regarding δ_{max} are related to premature failures, possibly induced by fabrication defects, or t_A variations to the expected design value induced during fabrication. The scatter in the values of γ_f is directly related to the δ_{max} variations.

Table 2 Tensile comparative evaluation between the Sikapower® 4720 and the Araldite® 2015 [30]

Properties	σ_f (MPa)	ε_f (%)	E (MPa)	σ_y (MPa)
SikaPower® 4720	27.519 ± 0.845	1.973 ± 0.343	2052.477 ± 84.818	23.286 ± 2.252
Araldite® 2015	21.63 ± 1.61	4.77 ± 0.15	1850 ± 210	12.63 ± 0.61

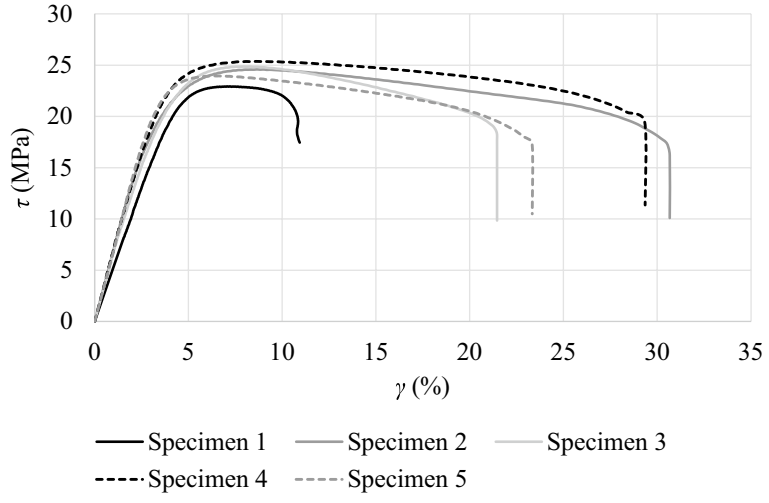

Fig. 8 τ–γ curves obtained for the five TAST tests

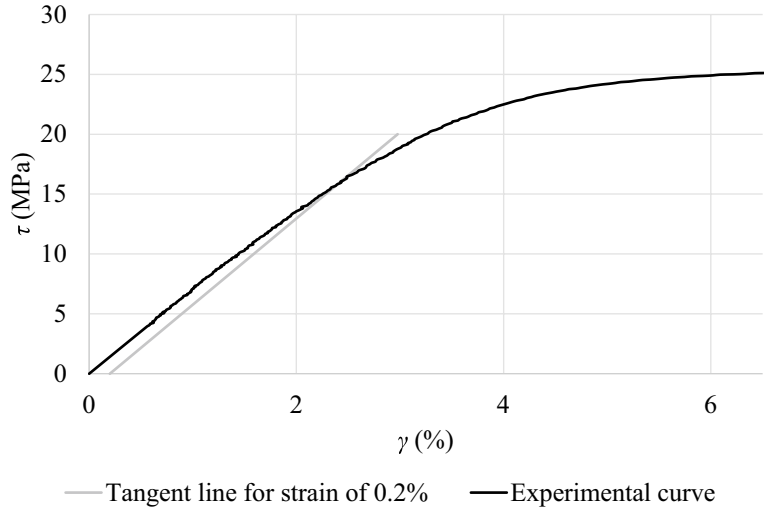

Fig. 9 Method to estimate τ_y for a single specimen, considering a line offset by $\gamma = 0.2$ %

Table 3 TAST mechanical properties in shear of the adhesive Sikapower® 4720

Specimen	P_{max} (N)	δ_{max} (mm)	τ_y (MPa)	τ_f (MPa)	γ_f (%)	G (MPa)
1	2865.967	0.071	15.213	22.928	10.936	697.567
2	3073.479	0.213	14.817	24.588	30.669	727.154
3	3108.062	0.142	13.539	24.864	21.460	770.566
4	3171.353	0.217	14.502	25.371	29.351	819.194
5	2994.543	0.149	16.309	23.956	23.333	739.212
Average	3042.681	0.159	14.876	24.341	23.150	750.738
Standard deviation	117.606	0.059	1.012	0.941	7.859	46.356

The TAST tests revealed a higher average value of τ_f than that provided by the manufacturer's sheet. Actually, the obtained value was 24.341 ± 0.941 MPa against an expected value of 14 MPa. However, the percentile standard deviation (3.9 %) is extremely low and all failures were cohesive, which validates the obtained results. It was not possible to compare γ_f because of absence of reference data. The obtained results revealed some scatter between specimens (23.150 ± 7.859 %), which is due to the difference in specimen 1. This value of γ_f clearly corresponds to a highly ductile adhesive. G measurements resulted in a value of 750.738 ± 46.356 MPa (percentile deviation of 6.2 %). Due to the isotropic nature of the adhesive, E and G can be used to obtain the Poisson's ratio (ν), which gave 0.367 and is in agreement with typical values for these adhesives. It was not possible to compare τ_y because of the lack of information. Table 4 evaluates the shear mechanical properties of the adhesive Sikapower® 4720 against the Araldite® 2015 [30]. All values of the Sikapower® 4720 overshoot those of the Araldite® 2015 except γ_f. Moreover, τ_y is much similar between both adhesives.

Tensile fracture tests

The P–δ curves of the six DCB tests are presented in Fig. 10. P initially increases linearly, as the energy stored in the specimen increases. When G_I reaches its critical value,

Table 4 Shear comparative evaluation between the Sikapower® 4720 and the Araldite® 2015 [30]

Properties	τ_f (MPa)	γ_f (%)	G (MPa)	υ	τ_y (MPa)
SikaPower® 4720	24.341 ± 0.941	23.150 ± 7.859	750.738 ± 46.356	0.367	14.876 ± 1.012
Araldite® 2015	17.9 ± 1.8	43.9 ± 3.4	560 ± 210	0.33[a]	14.6 ± 1.3

[a] Manufacturer's value

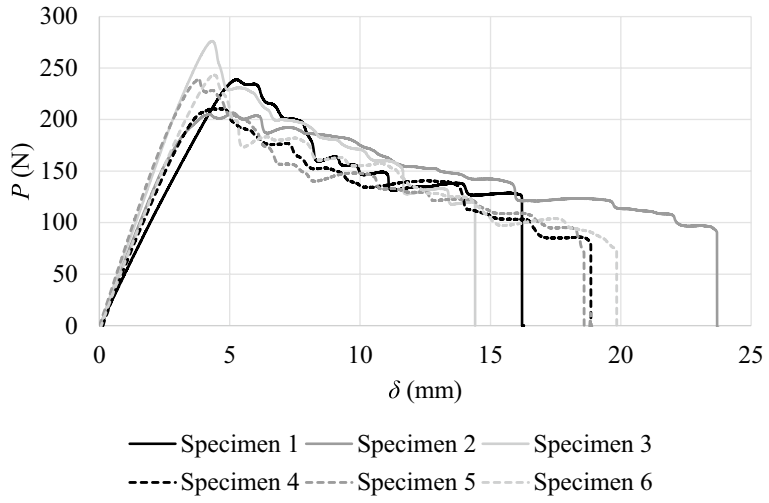

Fig. 10 *P–δ* curves for the DCB specimens

G_{Ic}, the crack starts to grow, and a reduction of P takes place because of the increasing bending moment induced by bigger a values. The curves of the several specimens showed a good correspondence, although with minor variations in the initial stiffness on account of different values of a_0. The R-curves were built from the P–δ curves following the previously mentioned data reduction methods, allowing to relate G_I with a or a_{eq} during the crack growth phase of each test [31]. Ideally, the R-curves are horizontal lines, although experimentally fluctuations may occur due to issues such as poor adhesive mixture, adhesion problems, defects and unstable crack growth. Figure 11 shows the R-curves by the different methods for a representative specimen of the DCB tests. It should be mentioned that, for the CCM, it is necessary to derive the $C = f(a)$ curve and to differentiate it. The $C = f(a)$ curve should span from the beginning of crack propagation up to the specimen's failure. For the particular specimen of Fig. 11, the R-curves are practically overlapped, resulting in consistent measurements of G_{Ic}. The CBBM has the advantage of not requiring the measurement of a, unlike happens with the CCM and CBT, which highly reduces the time required in the analysis and prevents errors in the measurement of a. The CCM still adds another source of error in the data analysis, because of the approximation taken in the calculation of dC/da, which is performed by taking the derivative of the $C = f(a)$ curve after fitting cubic polynomials [24]. After performing all the tests, fully cohesive failures were obtained for all DCB specimens. Table 5 summarizes the values of G_{Ic} by the different methods for all specimens, and also P_{max} and δ_{max} for each specimen. The G_{Ic} data is highly consistent for each specimen between

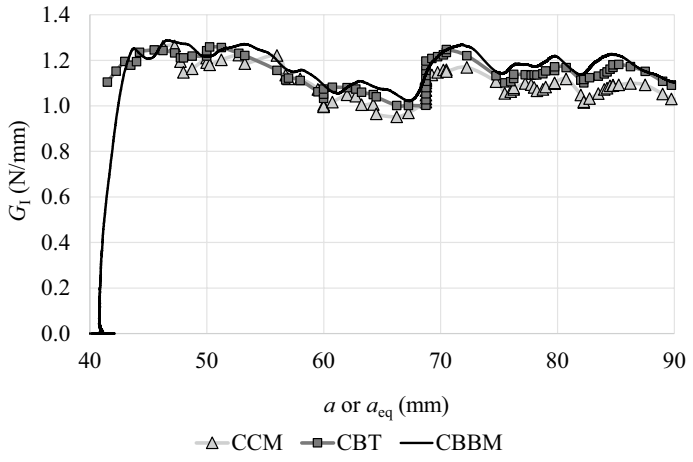

Fig. 11 CCM, CBT and CBBM *R*-curves for a DCB specimen

Table 5 Values of G_{Ic} obtained by the different data reduction methods from the DCB tests

Specimen	P_{max} (N)	δ_{max} (mm)	G_{Ic} (N/mm)		
			CCM	CBT	CBBM
1	238.825	16.287	1.249	1.317	1.363
2	206.584	23.846	1.395	1.443	1.401
3	276.072	14.413	1.350	1.447	1.598
4	210.687	19.150	1.059	1.174	1.186
5	239.236	19.022	1.067	1.120	1.173
6	243.150	19.948	1.084	1.168	1.040
Average	235.759	18.778	1.201	1.278	1.294
Standard deviation	23.025	2.958	0.138	0.132	0.182

methods, and between specimens of each method (small values of standard deviation). However, the G_{Ic} values of the CBBM were slightly higher than for the other methods. Nonetheless, this is regarded as the most robust method since it fully accounts for the FPZ and it is not affected by possible measurement errors of a.

After the analysis of all DCB specimens, no significant differences were found in the *R*-curves when comparing all considered data reduction methods. The measured values of G_{Ic} for each specimen were close between data reduction methods. No data is available from the manufacturer regarding this parameter. Evaluated against the CBBM, which is regarded as the most reliable method by not requiring measurement of a and including the FPZ effects in the results, the observed differences to the other methods were 7.2 % (CCM) and 1.2 % (CBT). Between specimens of the same method, the percentile deviations were 11.5 % (CCM), 10.3 % (CBT) and 14.1 % (CBBM). The current adhesive has $G_{Ic} = 1.294 \pm 0.182$ N/mm (CBBM values) compared to $G_{Ic} = 0.43 \pm 0.02$ N/mm of the Araldite® 2015 [30], which corresponds to an excess of nearly three times.

Shear fracture tests

Figure 12 compares the P–δ curves obtained in the eight ENF tests. For this particular test, eight specimens were considered to safeguard possible unstable crack propagations in some specimens, prone to occur in the ENF test. The general shape of the curves is in agreement between specimens, although one of these has a smaller elastic stiffness induced by a higher value of a_0. After P_{max} is attained, the load starts to decrease, which corresponds to the interest part of the ENF tests, in which G_{IIc} is measured. Afterwards, the load increases again when the FPZ reaches the vicinity of the loading cylinder. This portion of the curves was truncated because it is no longer valid for the measurement of G_{IIc}. Figure 13 compares the R-curves of a single specimen by the CCM, CBT and CBBM. In an identical manner to the DCB specimens, these R-curves correlate G_{II} with a or a_{eq} and their steady-state value during the crack propagation phase provides an estimation of G_{IIc}. For the specimen depicted in the figure, the valid crack propagation region ranged between $84 \leq a_{eq} \leq 92$ mm (CBBM curve). After this region, a gradual increase of G_{II} was found related to the FPZ reaching the loading cylinder and biasing the measured value of G_{IIc}. The full set of G_{IIc} values obtained by the three methods is shown in Table 6, together with the P_{max} and δ_{max} values for all specimens. The results for specimen 6 were discarded from the analysis due to a significant offset to the typical values obtained for the other specimens. Equally to the DCB results and owing to previous evidence regarding these methods [27], the CBBM is considered the most reliable.

In accordance with the previous tests, the ENF tests also revealed a high repeatability. The G_{IIc} results of each test agreed well between methods. Equally to G_{Ic}, comparison with reference values cannot be carried out. The percentile differences to the CBBM, once again considered the most robust method, are 3.3 % for the CCM and 22.9 % for the CBT. The discrepancy for the CBT is linked to the energy dissipated in

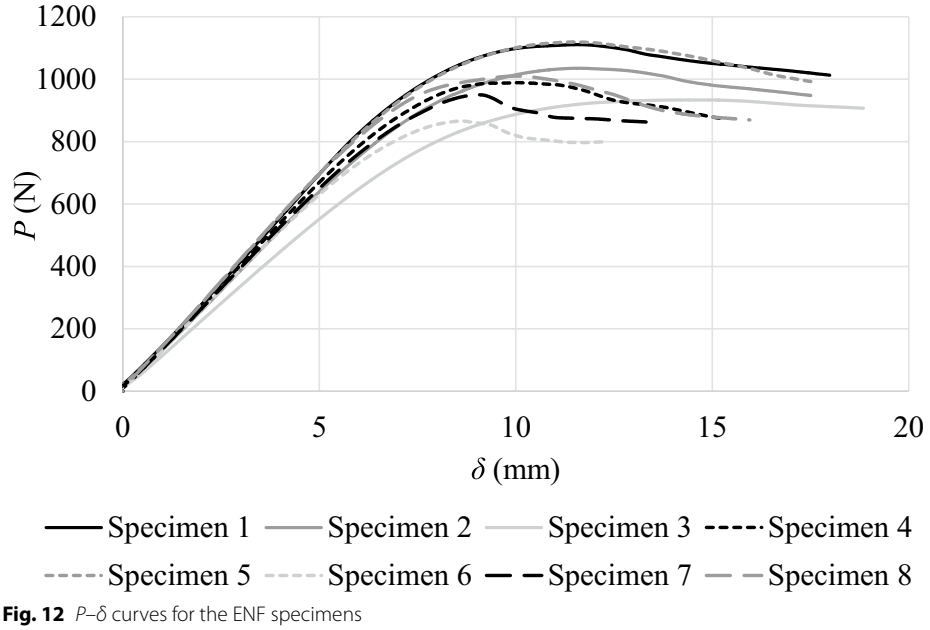

Fig. 12 *P*–*δ* curves for the ENF specimens

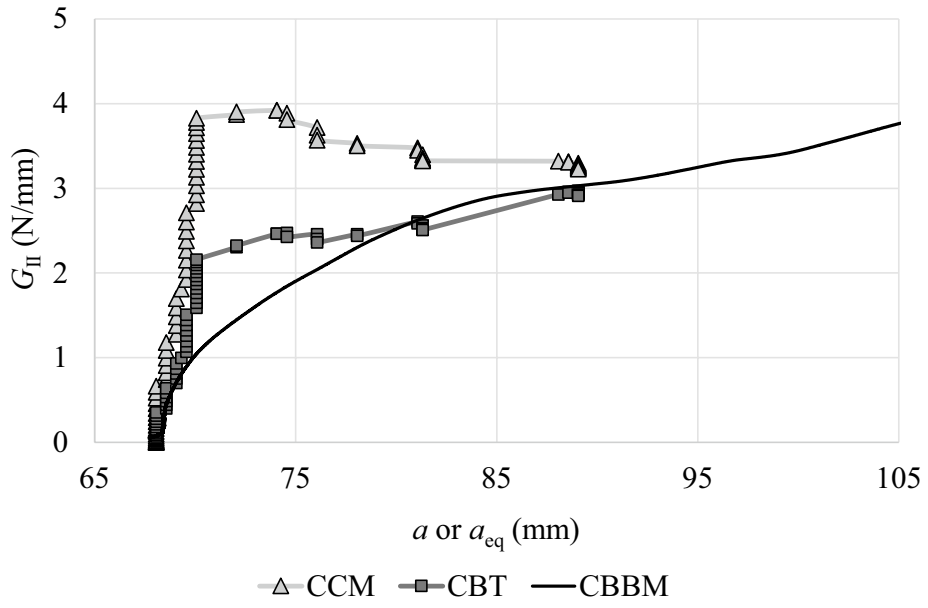

Fig. 13 CCM, CBT and CBBM *R*-curves for an ENF specimen

Table 6 Values of G_{IIc} obtained by the different data reduction methods from the ENF tests

Specimen	P_{max} (N)	δ_{max} (mm)	G_{IIc} (N/mm)		
			CCM	CBT	CBBM
1	1110.912	17.990	5.183	3.327	4.467
2	1035.342	17.507	4.473	3.886	4.544
3	933.773	18.847	3.729	3.858	4.327
4	989.140	15.350	4.671	2.824	4.151
5	1119.458	17.650	5.428	3.195	4.283
6	866.329	12.257	–	–	–
7	950.081	13.593	3.317	2.773	3.503
8	1010.304	15.953	3.843	2.984	4.367
Average	1001.917	16.143	4.378	3.264	4.235
Standard deviation	86.818	2.303	0.783	0.459	0.347

the FPZ, which is not accounted for in beam theories. Comparing the different specimens for each method, the percentile deviations were 17.9, 14.1 and 8.2 % for the CCM, CBT and CBBM, by this order. The CBBM results of the adhesive Sikapower® 4720 gave $G_{IIc} = 4.235 \pm 0.347$ N/mm, which is a slightly smaller value than that obtained for the Araldite® 2015, of $G_{IIc} = 4.70 \pm 0.34$ N/mm [30].

Conclusions

The main objective of this work was the complete mechanical and fracture characterization of a new epoxy adhesive (Sikapower® 4720). Bulk tensile and TAST tests were performed to obtain the tensile and shear mechanical properties, respectively. The bulk tensile tests gave the following values: $E = 2052.477 \pm 84.818$ MPa,

$\sigma_y = 23.286 \pm 2.252$ MPa, $\sigma_f = 27.519 \pm 0.845$ MPa, and $\varepsilon_f = 1.973 \pm 0.343$ %. From the manufacturer's data, only σ_f (24 MPa), E (1900 MPa) and ε_f (3 %) were available. The biggest difference was found in ε_f, justified by small experimental defects in the specimens that could compromise the full ductility of the specimens to develop. The TAST tests resulted in $G = 750.738 \pm 46.356$ MPa, $\tau_y = 14.876 \pm 1.012$ MPa, $\tau_f = 24.341 \pm 0.941$ and $\gamma_f = 23.150 \pm 7.859$ %. The only comparison with the manufacturer's data regards τ_f (14 MPa), which corresponds to a significant difference to the obtained value in this work. However, the manufacturer's value was empirically defined by the von Mises criterion which, as it is known, does not apply to toughened adhesives. The availability of E and G permits the calculation of ν for isotropic materials as 0.367, which is within the interval of expected values for structural adhesives, i.e., between 0.3 and 0.5 [1]. The G_{Ic} values, obtained by DCB tests, gave 1.201 ± 0.138 N/mm (CCM), 1.278 ± 0.132 N/mm (CBT) and 1.294 ± 0.182 N/mm (CBBM), corresponding to a good correspondence between methods. The ENF tests provided the G_{IIc} estimations as 4.378 ± 0.783 N/mm (CCM), 3.264 ± 0.459 N/mm (CBT) and 4.235 ± 0.347 N/mm (CBBM). As previously mentioned, the CBT under predicted the other methods. It was not possible to compare G_{Ic} and G_{IIc} with the manufacturer's values due to the absence of information. The comparison of the obtained results with the Araldite® 2015 revealed better properties in all parameters except ε_f, γf and G_{IIc}, in this last parameter by a very short difference.

Authors' contributions

JPRM—carried out the experimental tests and analyses. RDSG, EASM and LFMS wrote the manuscript. All authors read and approved the final manuscript.

Author details

[1] Departamento de Engenharia Mecânica, Instituto Superior de Engenharia do Porto, Instituto Politécnico do Porto, Rua Dr. António Bernardino de Almeida, 431, 4200-072 Porto, Portugal. [2] Instituto de Ciência e Inovação em Engenharia Mecânica e Engenharia Industrial (INEGI), Rua Dr. Roberto Frias, 4200-465 Porto, Portugal. [3] Departamento de Engenharia Mecânica, Faculdade de Engenharia, Universidade do Porto, Rua Dr. Roberto Frias, 4200-465 Porto, Portugal.

Acknowledgements

The authors would like to thank Sika® Portugal for supplying the adhesive Sikapower® 4720.

Competing interests

The authors declare that they have no competing interests.

Received: 17 November 2015 Accepted: 14 December 2015
Published online: 22 December 2015

References

1. Silva LFM, Öchsner A, Adams RD. Handbook of adhesion technology. 1st ed. Berlin: Springer; 2011.
2. Needleman A. A continuum model for void nucleation by inclusion debonding. J Appl Mech. 1987;54:525–31.
3. Tvergaard V, Hutchinson JW. The relation between crack growth resistance and fracture process parameters in elastic–plastic solids. J Mech Phys Solids. 1992;40:1377–97.
4. Camacho GT, Ortiz M. Computational modelling of impact damage in brittle materials. Int J Solids Struct. 1996;33:2899–938.
5. Banea MD, da Silva LFM, Campilho RDSG. Effect of temperature on the shear strength of aluminium single lap bonded joints for high temperature applications. J Adhes Sci Technol. 2014;28:1367–81.
6. ISO 527-5 Standard. 1997. Plastics—determination of tensile properties. Geneva, Switzerland.
7. ASTM D638-03 Standard. 2014. Standard test method for tensile properties of plastics. West Conshohocken, USA.
8. ISO 11003-2 Standard. 1993. Adhesives—determination of shear behaviour of structural bonds—part 2: thick-adherend tensile-test method. Geneva, Switzerland.
9. ASTM E143-02 Standard. 2013. Standard test method for shear modulus at room temperature. West Conshohocken, USA.
10. ISO 25217 Standard. 2009. Adhesives—determination of the mode 1 adhesive fracture energy of structural adhesive joints using double cantilever beam and tapered double cantilever beam specimens. Geneva, Switzerland.
11. Kanninen MF, Popelar CH. Advanced fracture mechanics. Oxford: Oxford University Press; 1985.
12. Ding W. 1999. Delamination analysis of composite laminates. PhD Thesis. University of Toronto, Canada.

13. Robinson P, Das S. Mode I DCB testing of composite laminates reinforced with z-direction pins: a simple model for the investigation of data reduction strategies. Eng Fract Mech. 2004;71:345–64.
14. de Moura MFSF, Campilho RDSG, Gonçalves JPM. Crack equivalent concept applied to the fracture characterization of bonded joints under pure mode I loading. Compos Sci Technol. 2008;68:2224–30.
15. de Moura MFSF, Gonçalves JPM, Chousal JAG, Campilho RDSG. Cohesive and continuum mixed-mode damage models applied to the simulation of the mechanical behaviour of bonded joints. Int J Adhes Adhes. 2008;28:419–26.
16. Saldanha DFS, Canto C, da Silva LFM, Carbas RJC, Chaves FJP, Nomura K, Ueda T. Mechanical characterization of a high elongation and high toughness epoxy adhesive. Int J Adhes Adhes. 2013;47:91–8.
17. García JA, Chiminelli A, García B, Lizaranzu M, Jiménez MA. Characterization and material model definition of toughened adhesives for finite element analysis. Int J Adhes Adhes. 2011;31:182–92.
18. Jin H, Miller GM, Pety SJ, Griffin AS, Stradley DS, Roach D, Sottos NR, White SR. Fracture behavior of a self-healing, toughened epoxy adhesive. Int J Adhes Adhes. 2013;44:157–65.
19. Kim BC, Park SW, Lee DG. Fracture toughness of the nano-particle reinforced epoxy composite. Compos Struct. 2008;86:69–77.
20. NF T 76-142 Standard. 1988. Méthode de préparation de plaques d'adhésifs structuraux pour la réalisation d'éprouvettes d'éssai de caractérisation. La Plaine Saint-Denis. France.
21. Pinto SDM. 2013. Determinação das propriedades mecânicas à tração de adesivos estruturais frágeis e dúcteis. MSc Thesis. Instituto superior de Engenharia do Porto, Porto.
22. Morais JFA. 2013. Desenvolvimento de ferramentas e provetes para o ensaio thick adherend shear test (TAST). MSc Thesis. Instituto superior de Engenharia do Porto, Porto.
23. Campilho RDSG, Banea MD, Pinto AMG, da Silva LFM, de Jesus AMP. Strength prediction of single- and double-lap joints by standard and extended finite element modelling. Int J Adhes Adhes. 2011;31:363–72.
24. Banea MD, da Silva LFM, Campilho RDSG. Effect of temperature on tensile strength and mode I fracture toughness of a high temperature epoxy adhesive. J Adhes Sci Technol. 2012;26:939–53.
25. ISO 15024 Standard. 2011. Fibre-reinforced plastic composites—determination of mode I interlaminar fracture toughness, GIC, for unidirectionally reinforced materials. Geneva, Switzerland.
26. Campilho RDSG, Moura DC, Gonçalves DJS, da Silva JFMG, Banea MD, da Silva LFM. Fracture toughness determination of adhesive and co-cured joints in natural fibre composites. Compos Part B Eng. 2013;50:120–6.
27. de Moura MFSF, Campilho RDSG, Gonçalves JPM. Pure mode II fracture characterization of composite bonded joints. Int J Solids Struct. 2009;46:1589–95.
28. Compston P, Jar PYB, Burchill PJ, Takahashi K. The effect of matrix toughness and loading rate on the mode-II interlaminar fracture toughness of glass-fibre/vinyl-ester composites. Compos Sci Technol. 2001;61:321–33.
29. Wang Y, Williams JG. Corrections for mode II fracture toughness specimens of composite materials. Compos Sci Technol. 1992;43:251–6.
30. Campilho RDSG, Banea MD, Neto JABP, da Silva LFM. Modelling adhesive joints with cohesive zone models: effect of the cohesive law shape of the adhesive layer. Int J Adhes Adhes. 2013;44:48–56.
31. Shahverdi M, Vassilopoulos AP, Keller T. Modeling effects of asymmetry and fiber bridging on Mode I fracture behaviour of bonded pultruded composite joints. Eng Fract Mech. 2013;99:335–48.